Energy Materials

Supplementary Materials

First-principles investigation of topological vanadium chalcogenide monolayers for synergistic sodium storage and sulfur conversion

Awais Ghani[1,*], Shehzad Ahmed[2,*], Muhammad Bilal[3], Adil Murtaza[4], Hongliang Du[1], Imran Muhammad[5,*]

[1]Multifunctional Electronic Ceramics Laboratory, College of Engineering, Xi'an International University, Xi'an 710077, Shaanxi, China.
[2]China-UK Low Carbon College, Shanghai Jiao Tong University, Shanghai 201306, China.
[3]Department of Mathematics and Industrial Engineering, Polytechnique Montréal, Montréal H3T 1J4, Canada.
[4]Guangdong Provincial Key Laboratory of Sensing Physics and System Integration Applications, School of Physics and Optoelectronic Engineering, Guangdong University of Technology, Guangzhou 510006, Guangdong, China.
[5]School of Energy, National Industry-Education Platform of Energy Storage, Tianjin University, Tianjin 300350, China.

[*]**Correspondence to:** Dr. Awais Ghani, Multifunctional Electronic Ceramics Laboratory, College of Engineering, Xi'an International University, Xi'an 710077, Shaanxi, China. E-mail: awaisghani@xaiu.edu.cn; Dr. Shehzad Ahmed, China-UK Low Carbon College, Shanghai Jiao Tong University, Shanghai 201306, China. E-mail: shehzadahmed@sjtu.edu.cn; Dr. Imran Muhammad, School of Energy, National Industry-Education Platform of Energy Storage, Tianjin University, Tianjin 300350, China. E-mail: imrankhan25@tju.edu.cn

CONTENTS

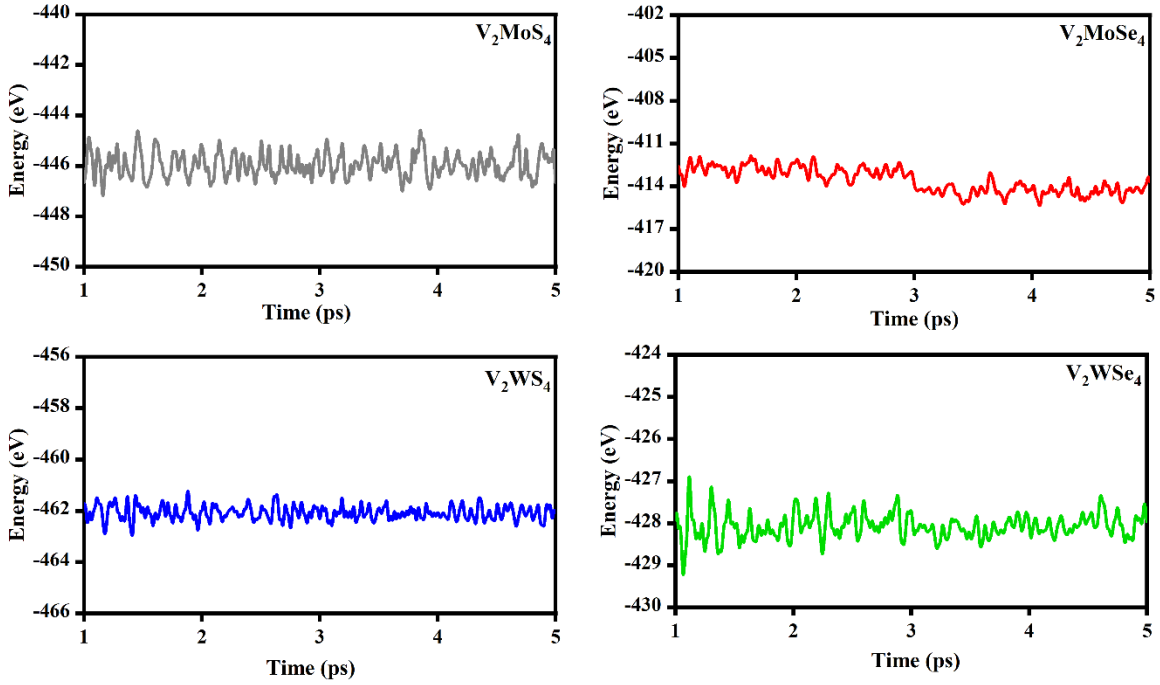

Figure S1. AIMD simulations of V_2AB_4 (A = Mo, W; B = S, Se) monolayers at 500 K for 5 ps.

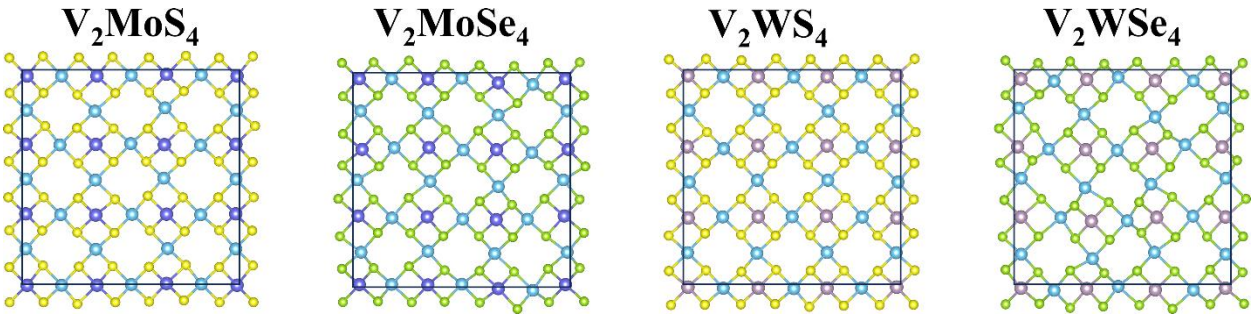

Figure S2. Atomic structures of V_2AB_4 (A = Mo, W; B = S, Se) monolayers after AIMD simulations at 300 K for 5 ps.

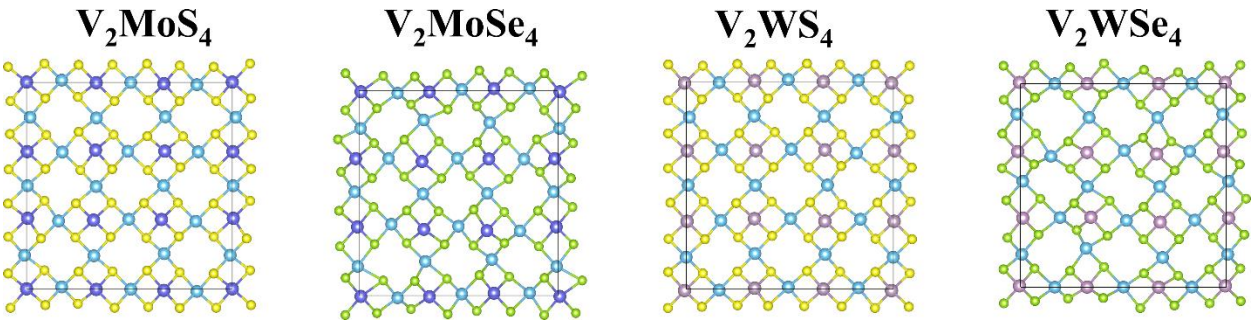

Figure S3 Atomic structures of V_2AB_4 (A = Mo, W; B = S, Se) monolayers after AIMD simulations at 500 K for 5 ps.

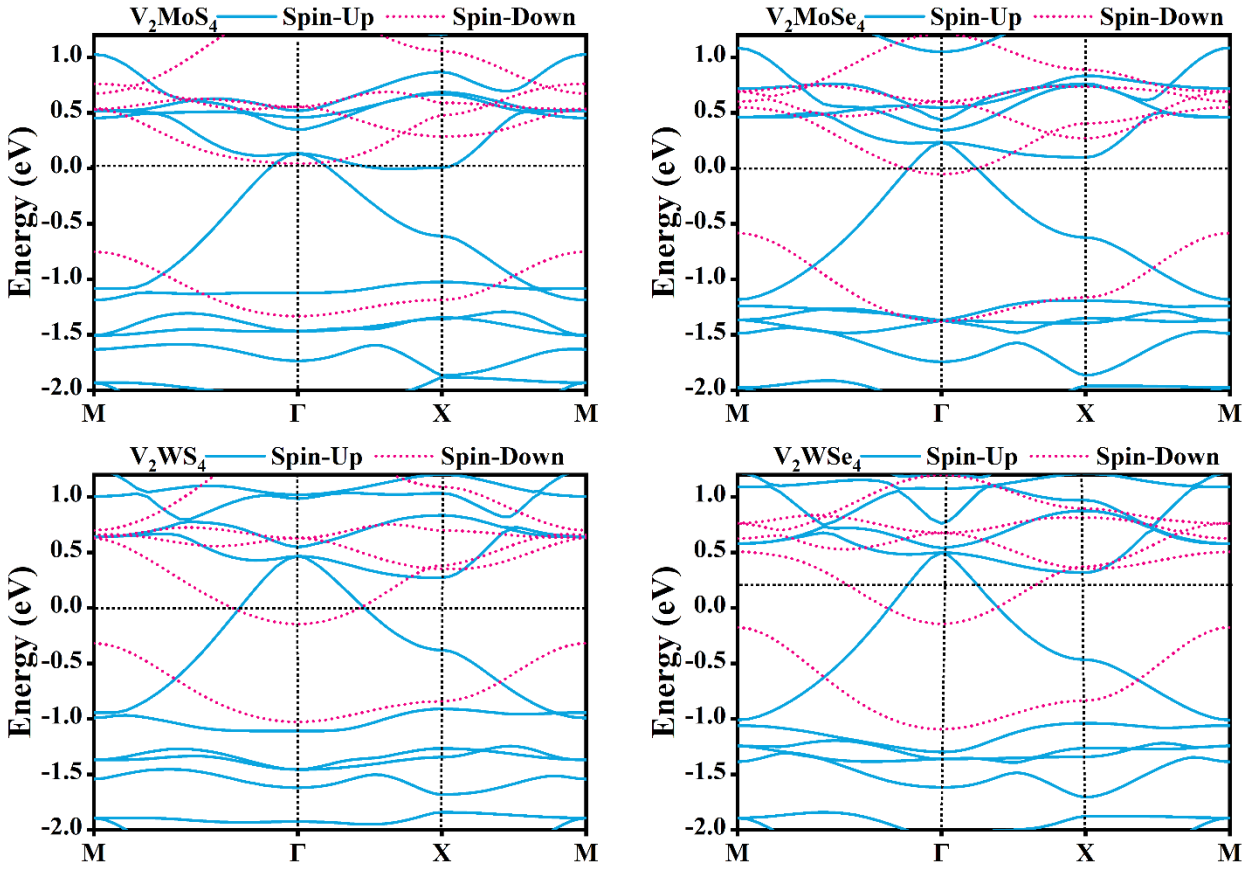

Figure S4. Band structures of V_2AB_4 (A = Mo, W; B = S, Se) monolayers without spin–orbit coupling.

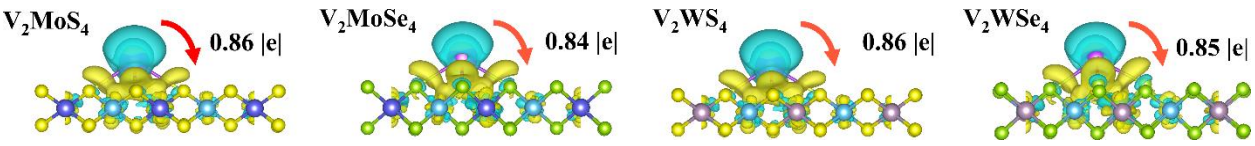

Figure S5. Charge density difference for a single K ion adsorbed on V_2AB_4 (A = Mo, W; B = S, Se) monolayers. Yellow and cyan isosurfaces represent electron accumulation and depletion, respectively, with an isosurface value of 0.002 e $Å^{-3}$. The numerical values indicate the amount of charge transferred from the K ion to the host monolayer, obtained from Bader charge analysis.

›

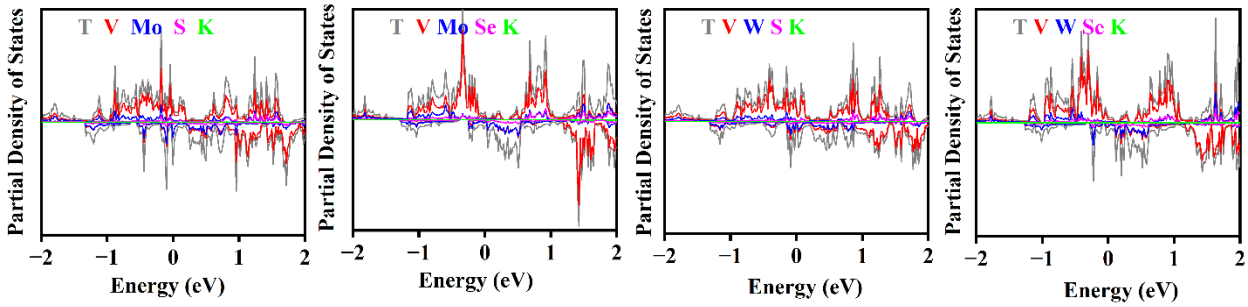

Figure S6. Partial densities of states of a single K ion adsorbed on V_2AB_4 (A = Mo, W; B = S, Se) monolayers.

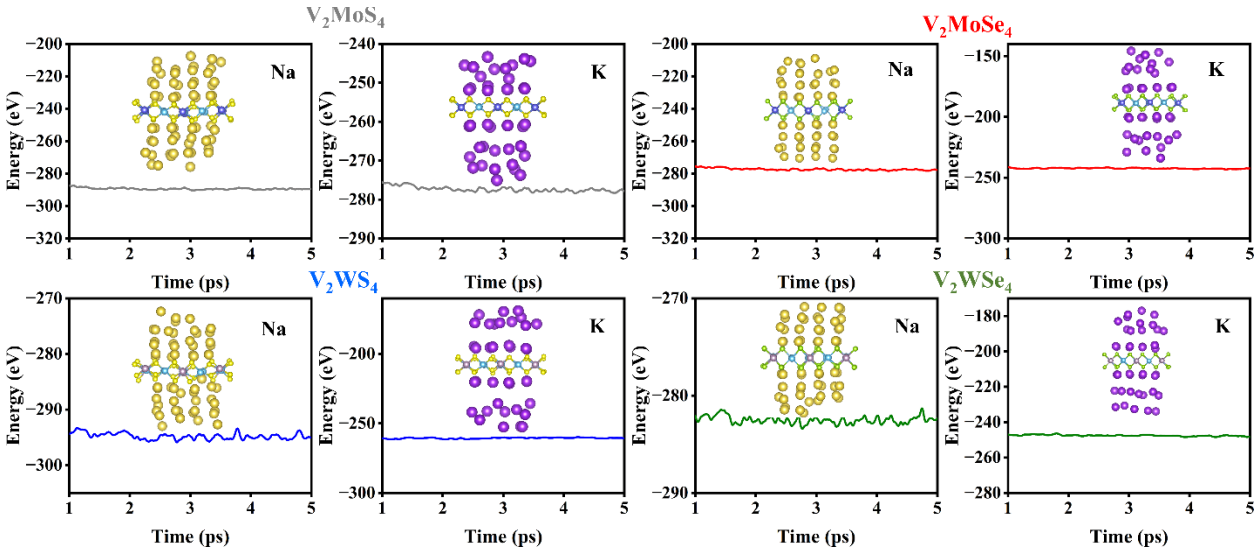

Figure S7. AIMD energy profiles and corresponding configurations of fully adsorbed Na and K ions on V_2AB_4 (A = Mo, W; B = S, Se) monolayers at 300 K for 5 ps.

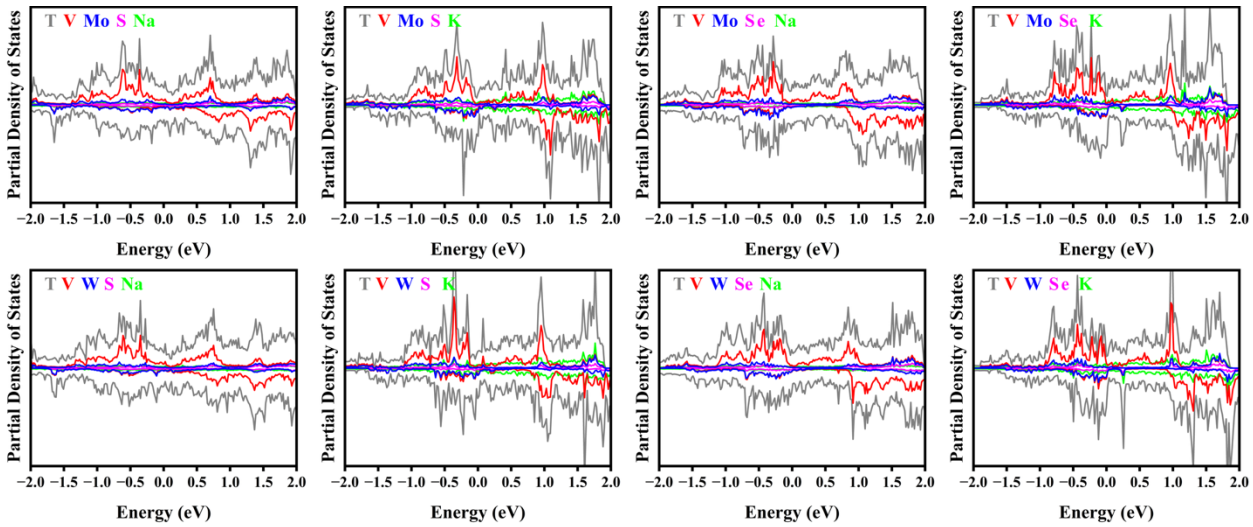

Figure S8. Partial densities of states of fully adsorbed Na/K ions on V_2AB_4 (A = Mo, W; B = S, Se) monolayers.

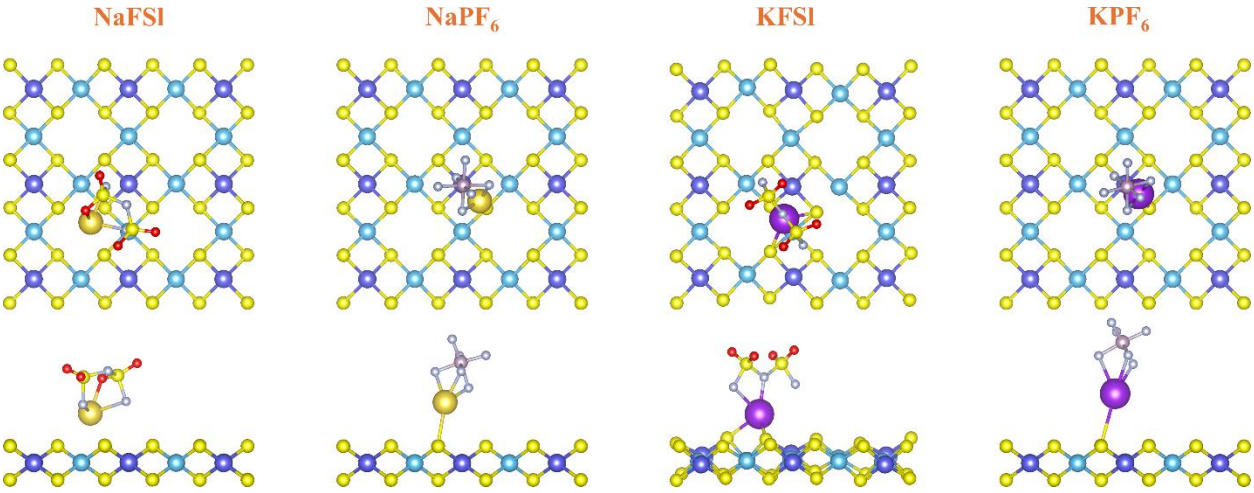

Figure S9. Optimized adsorption configurations of NaFSI, $NaPF_6$, KFSI, and KPF_6 on the V_2MoS_4 monolayer, showing top and side views.

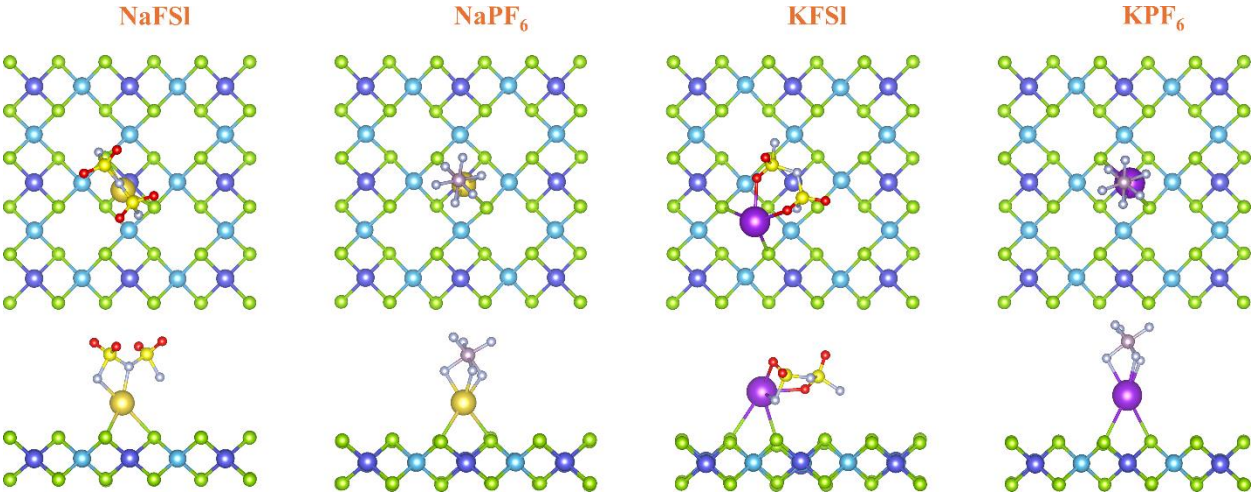

Figure S10. Optimized adsorption configurations of NaFSI, $NaPF_6$, KFSI, and KPF_6 on the V_2MoSe_4 monolayer, showing top and side views.

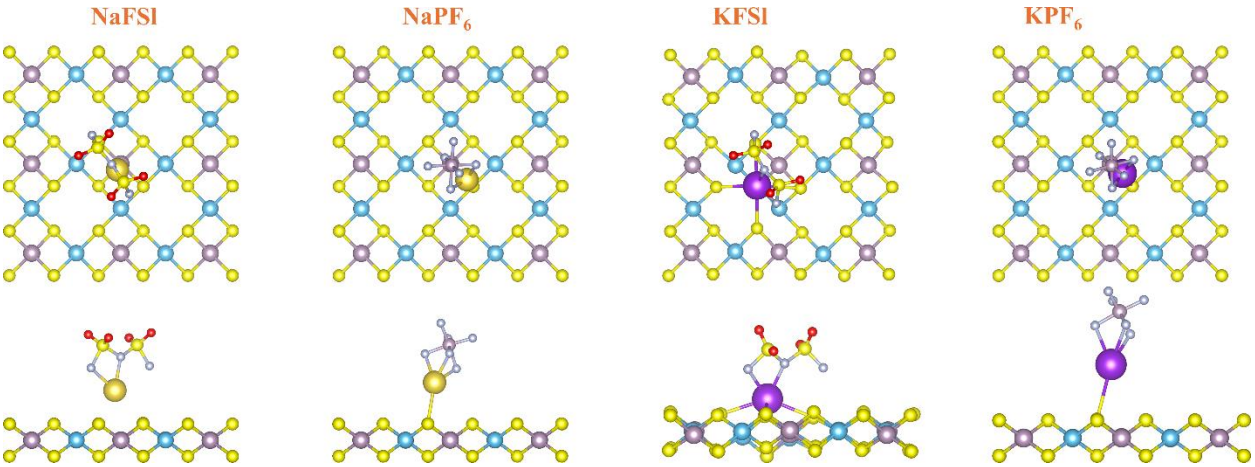

Figure S11. Optimized adsorption configurations of NaFSI, $NaPF_6$, KFSI, and KPF_6 on the V_2WS_4 monolayer, showing top and side views.

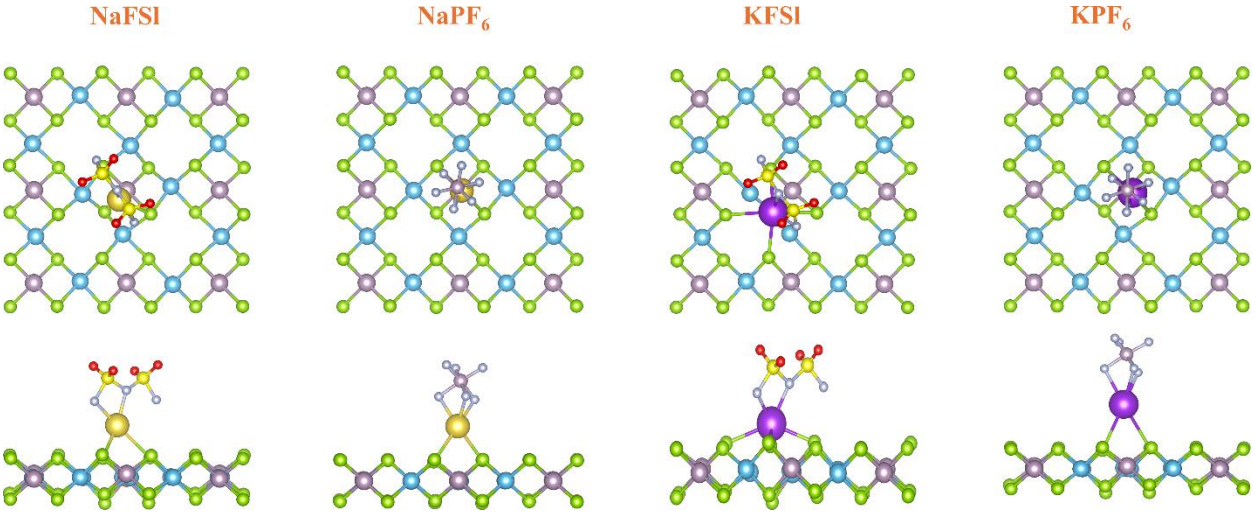

Figure S12. Optimized adsorption configurations of NaFSI, $NaPF_6$, KFSI, and KPF_6 on the V_2WSe_4 monolayer, showing top and side views.

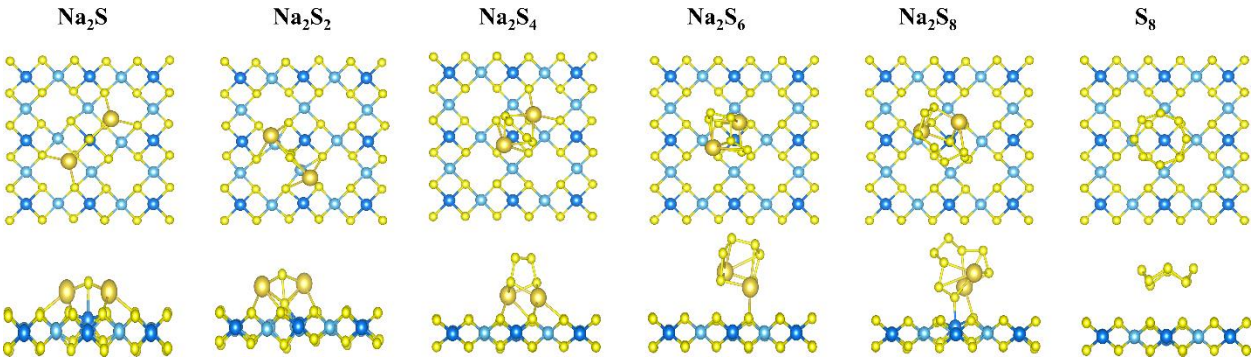

Figure S13. Optimized adsorption configurations of Na_2S_n (n = 1, 2, 4, 6, and 8) and S_8 clusters on the V_2MoS_4 monolayer, showing top and side views.

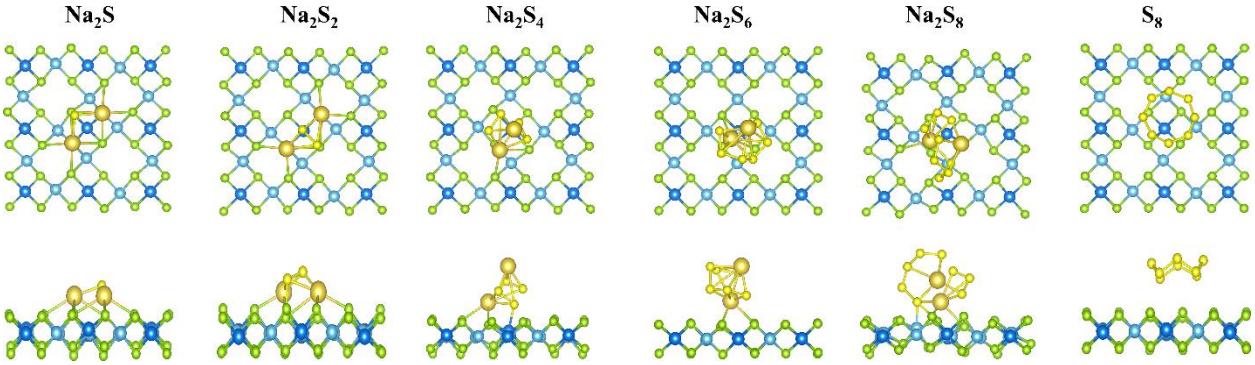

Figure S14. Optimized adsorption configurations of Na_2S_n (n = 1, 2, 4, 6, and 8) and S_8 clusters on the V_2MoSe_4 monolayer, showing top and side views.

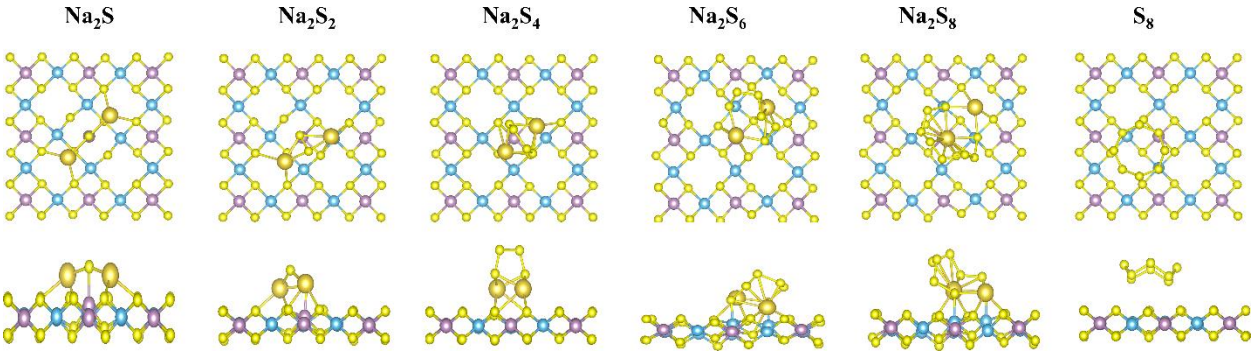

Figure S15. Optimized adsorption configurations of Na_2S_n (n = 1, 2, 4, 6, and 8) and S_8 clusters on the V_2WS_4 monolayer, showing top and side views.

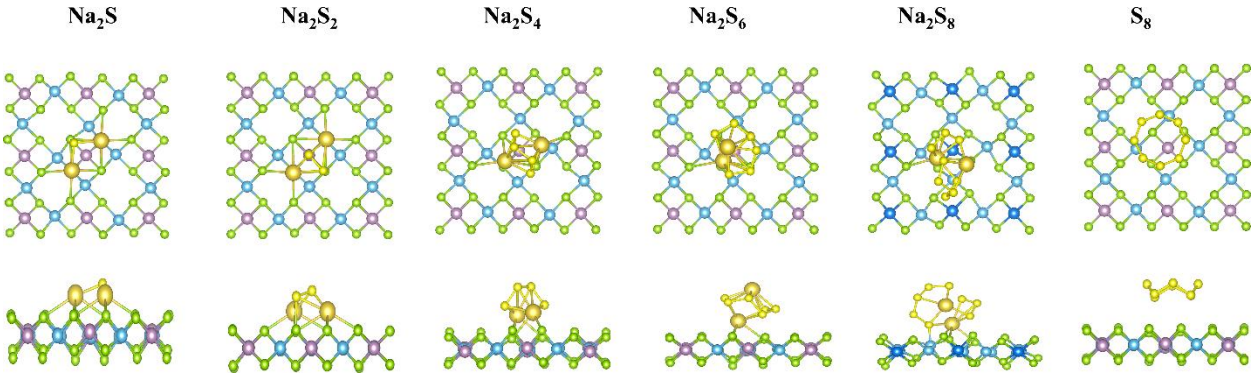

Figure S16. Optimized adsorption configurations of Na_2S_n (n = 1, 2, 4, 6, and 8) and S_8 clusters on the V_2WSe_4 monolayer, showing top and side views.

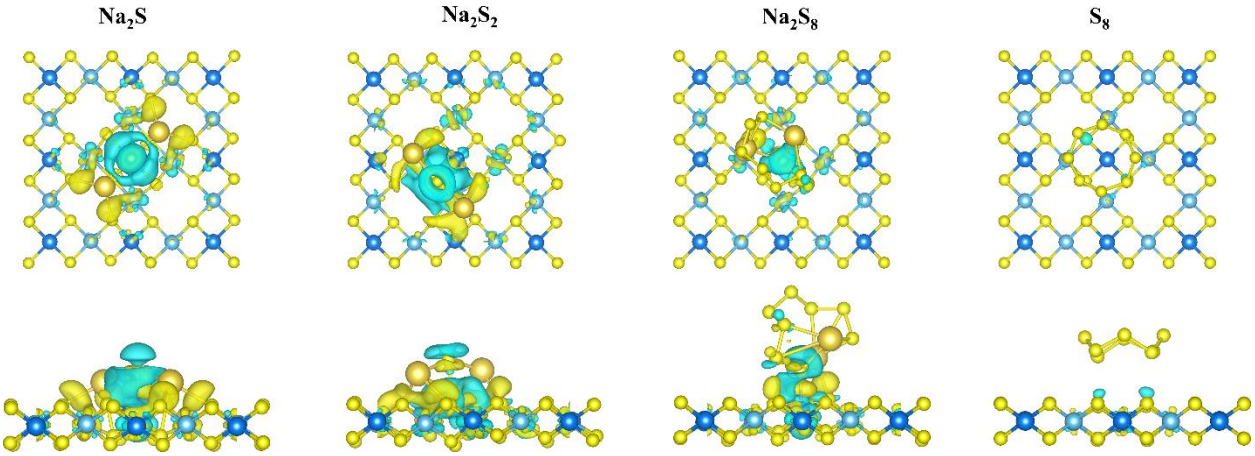

Figure S17. Charge-density-difference distributions of Na_2S, Na_2S_2, Na_2S_8, and S_8 adsorbed on the V_2MoS_4 monolayer. The upper and lower rows show the top and side views, respectively. Yellow and cyan isosurfaces denote electron gain and electron loss, respectively, at an isosurface value of 0.002 e $Å^{-3}$.

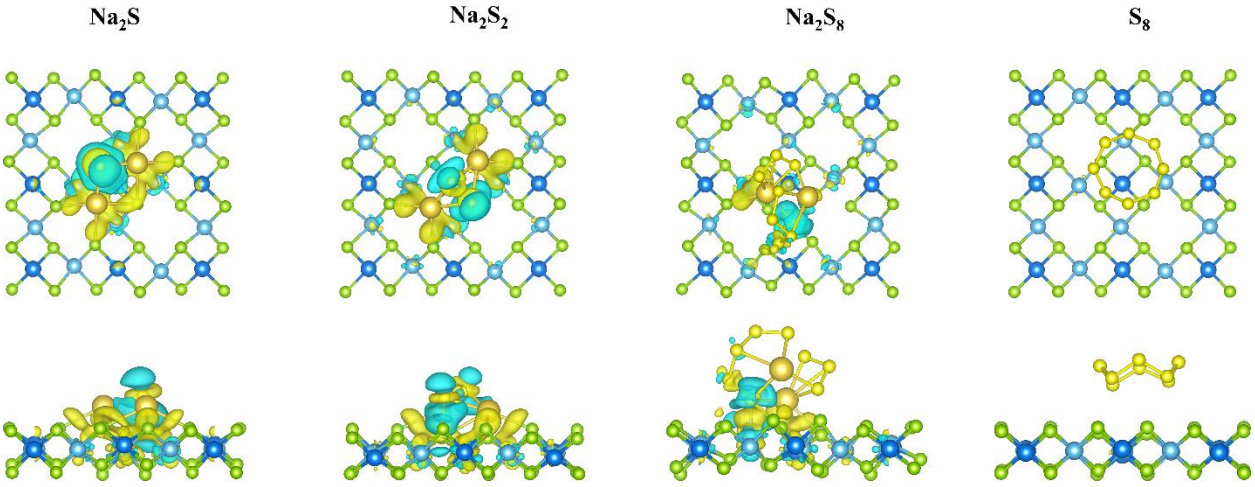

Figure S18. Charge-density-difference distributions of Na_2S, Na_2S_2, Na_2S_8, and S_8 adsorbed on the V_2MoSe_4 monolayer. The upper and lower rows show the top and side views, respectively. Yellow and cyan isosurfaces denote electron gain and electron loss, respectively, at an isosurface value of 0.002 e $Å^{-3}$.

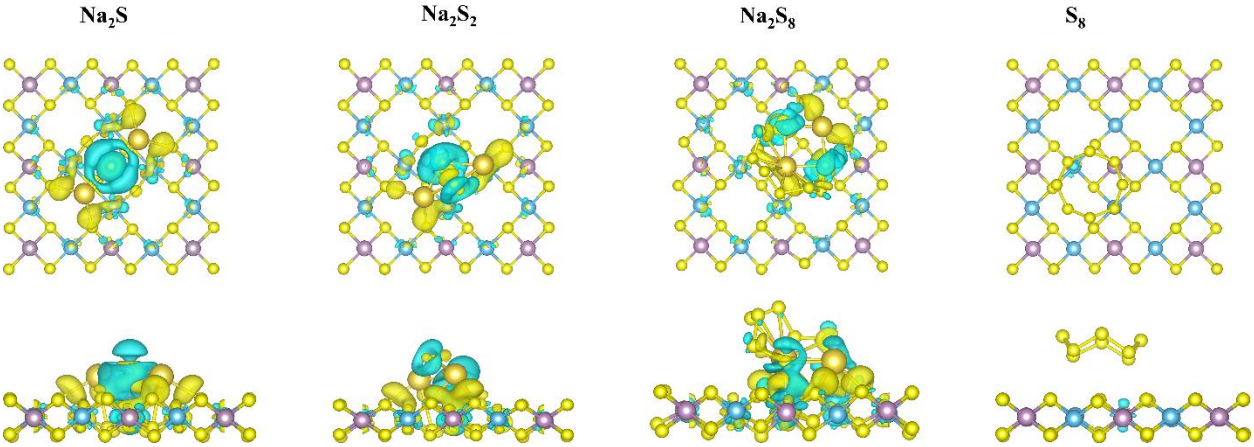

Figure S19. Charge-density-difference distributions of Na_2S, Na_2S_2, Na_2S_8, and S_8 adsorbed on the V_2WS_4 monolayer. The upper and lower rows show the top and side views, respectively. Yellow and cyan isosurfaces denote electron gain and electron loss, respectively, at an isosurface value of 0.002 e $Å^{-3}$.

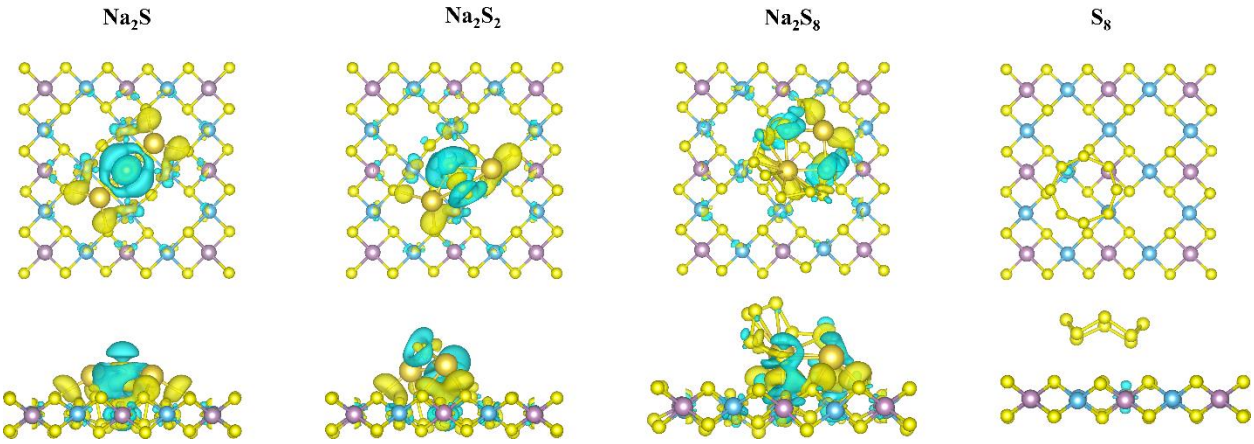

Figure S20. Charge-density-difference distributions of Na_2S, Na_2S_2, Na_2S_8, and S_8 adsorbed on the V_2WSe_4 monolayer. The upper and lower rows show the top and side views, respectively. Yellow and cyan isosurfaces denote electron gain and electron loss, respectively, at an isosurface value of 0.002 e $Å^{-3}$.

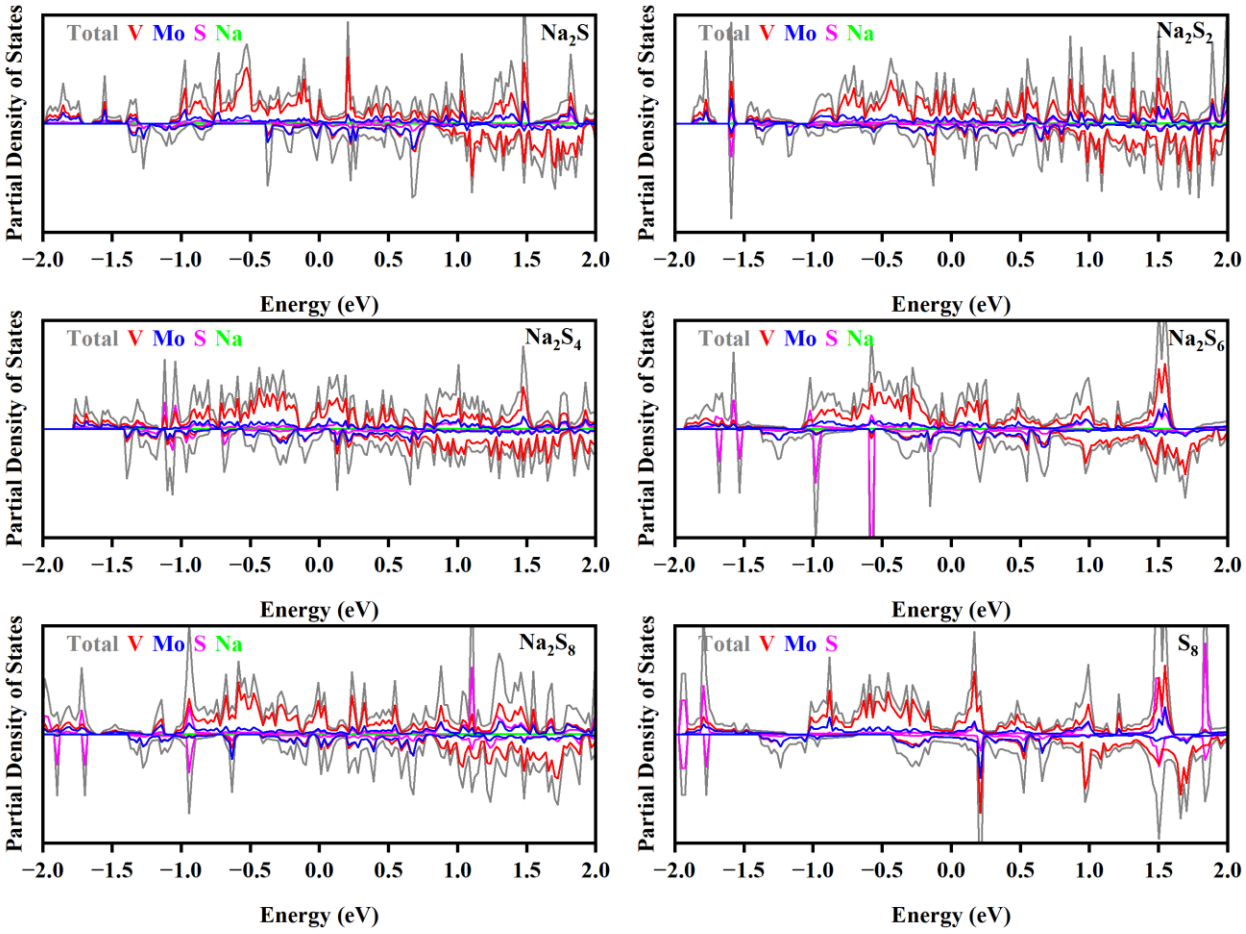

Figure S21. Spin-polarized PDOS of Na_2S_n (n = 1, 2, 4, 6, and 8) and S_8 adsorbed on the V_2MoS_4 monolayer.

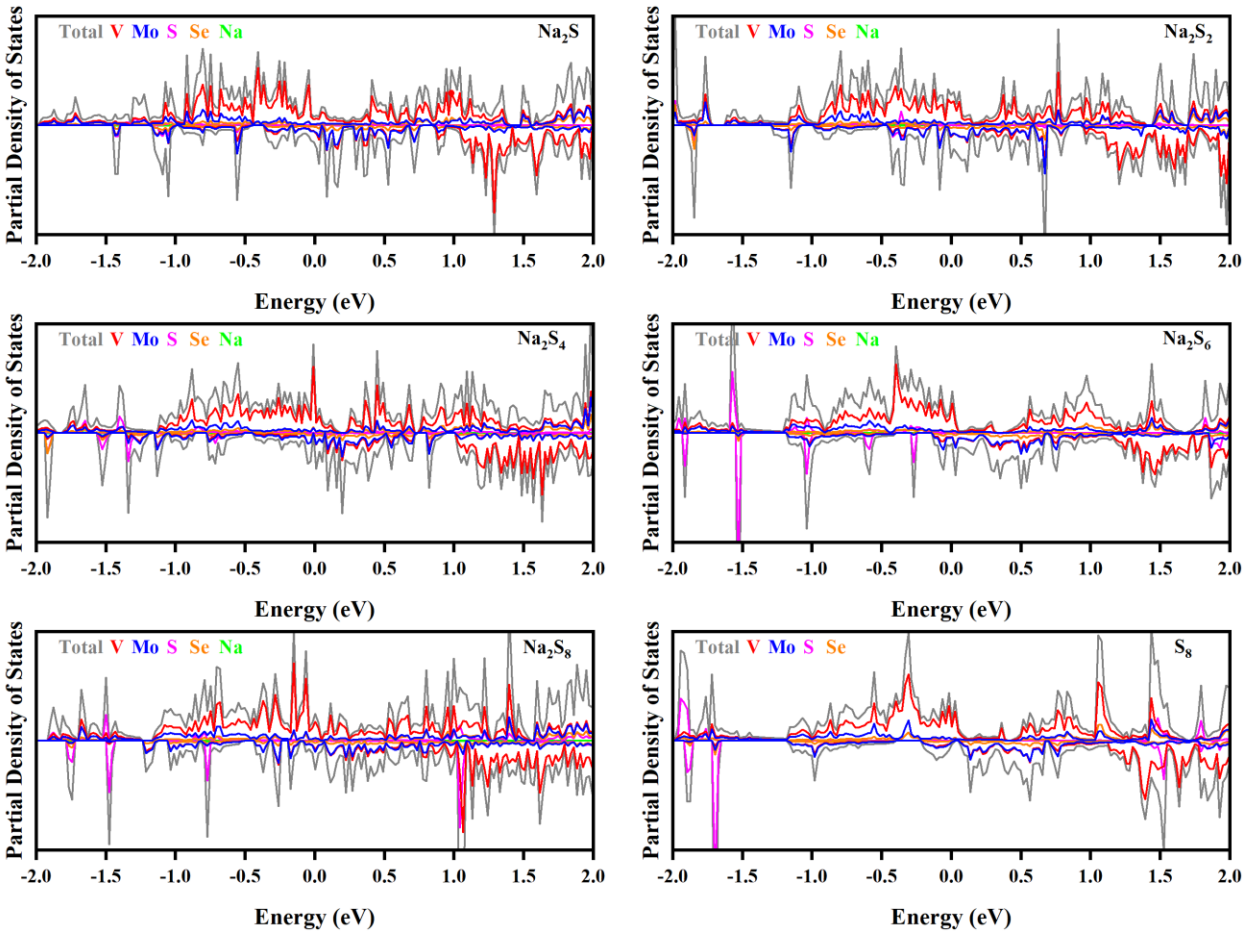

Figure S22. Spin-polarized PDOS of Na_2S_n (n = 1, 2, 4, 6, and 8) and S_8 adsorbed on the V_2MoSe_4 monolayer

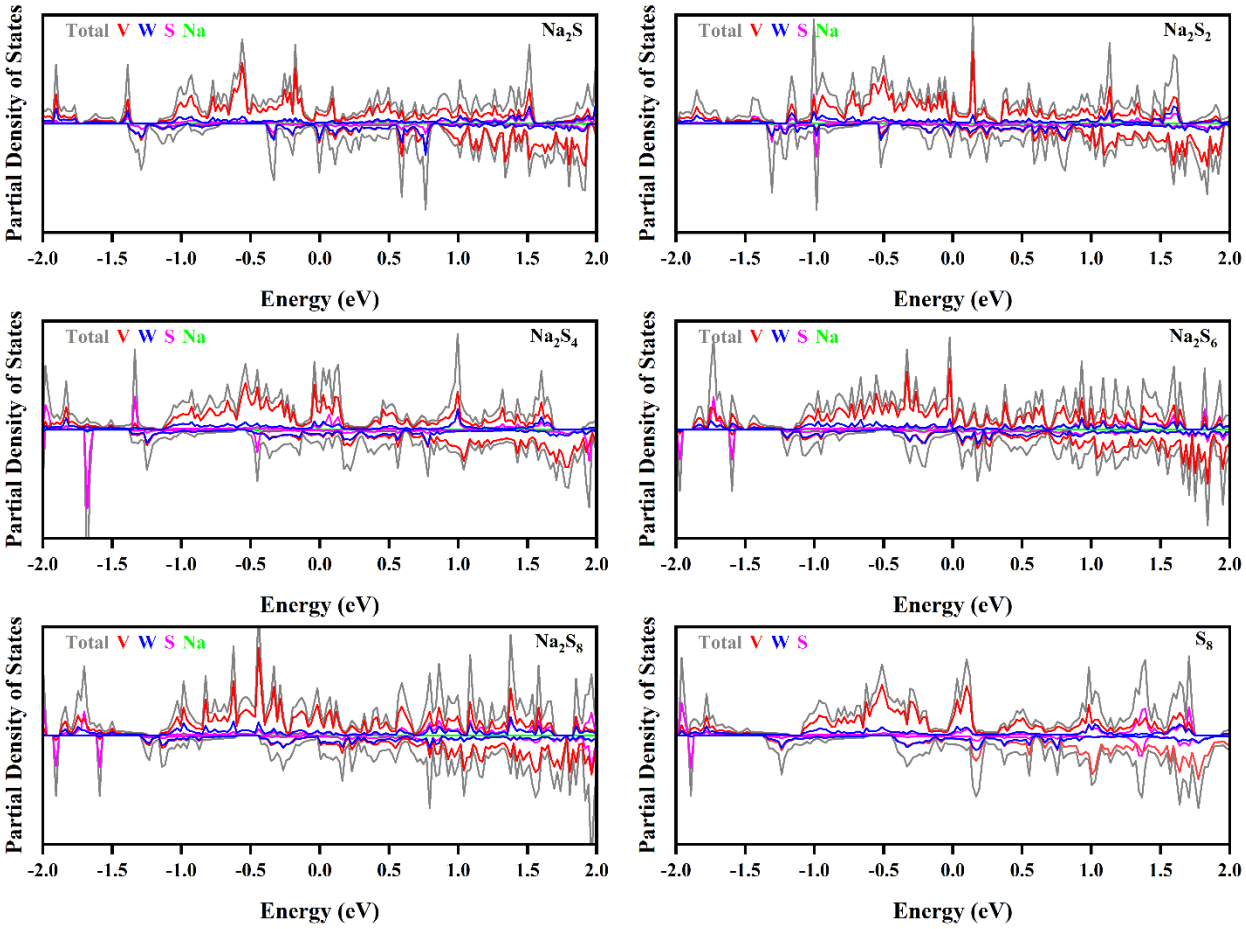

Figure S23. Spin-polarized PDOS of Na_2S_n (n = 1, 2, 4, 6, and 8) and S_8 adsorbed on the V_2WS_4 monolayer

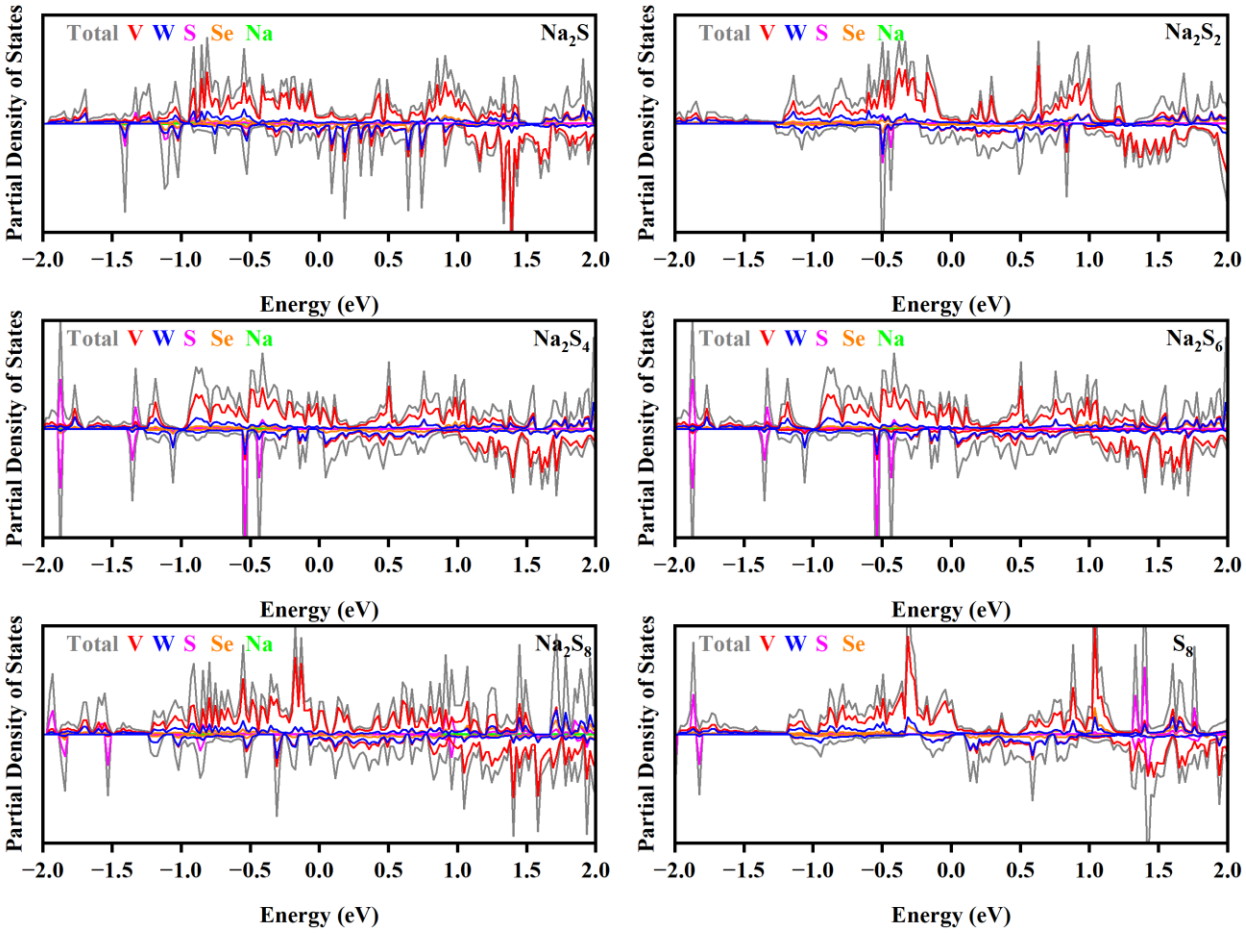

Figure S24. Spin-polarized PDOS of Na_2S_n (n = 1, 2, 4, 6, and 8) and S_8 adsorbed on the V_2WSe_4 monolayer.